IEEE Access
Multidisciplinary | Rapid Review | Open Access Journal

Received November 13, 2019, accepted November 25, 2019, date of publication December 3, 2019,
date of current version December 17, 2019.

Digital Object Identifier 10.1109/ACCESS.2019.2957274

Extended Sliding Mode Disturbance Observer-Based Sensorless Control of IPMSM for Medium and High-Speed Range Considering Railway Application

ABEBE TEKLU WOLDEGIORGIS[1,2], (Student Member, IEEE), XINGLAI GE[1], (Member, IEEE), SONGTAO LI[1], AND MANNAN HASSAN[1]

[1]Key Laboratory of Magnetic Suspension Technology and Maglev Vehicle, Ministry of Education, Southwest Jiaotong University, Chengdu 611756, China
[2]Addis Ababa Institute of Technology, Addis Ababa University, Addis Ababa 1176, Ethiopia

Corresponding author: Abebe Teklu Woldegiorgis (abebe.teklu@aait.edu.et)

This work was supported by the National Natural Science Foundation of China under Grant 51677156 and Grant 61733015.

ABSTRACT The sliding mode observer (SMO)-based approach known for its robustness towards parameter variation (external disturbance) has been used for the sensorless motor drive system. Delay compensation is commonly added to overcome the phased delay resulted from the introduction of the low-pass filter for chattering suppression. In this paper, a new extended sliding mode disturbance observer (ESMDO)-based sensorless control of interior permanent magnet synchronous motor for the medium and high-speed range is presented. The effect of parameter variation and coordinate transformation is considered as a lumped disturbance, and ESMDO is designed to compensate for the imminent impact of such scenarios. A Lyapunov stability theory is adopted to guarantee the stability of the proposed ESMDO-based sensorless control method. The ESMDO has an inbuilt low-pass filter and does not introduce a phased delay. A very large load change/reference speed variation may result in system instability or require higher controller gains that lead to system chattering. Hence, a PI-based compensation is incorporated to achieve a smooth and robust sensorless control algorithm considering the d-axis disturbance. Finally, extensive simulation and hardware-in-the-loop (HIL) test using the TMS320F28335 control unit in a real-time environment are conducted to verify the effectiveness of the proposed sensorless control method.

INDEX TERMS Extended sliding mode disturbance observer (ESMDO), IPMSM, sensorless control, traction drive.

I. INTRODUCTION

Squirrel-cage asynchronous machines are the most widely used traction motors for railway applications. However, the demand for high power, low environmental pollution, and volume reduction enforce the development of new traction motors. Interior permanent magnet synchronous motor (IPMSM) happened to be a solution to this problem due to its high power to weight ratio, low generated noise, low maintenance, low torque ripple, and the possibility of an enclosed system (less heat generation) [1]–[4]. Consequently, IPMSM is increasingly popular in urban rail transit.

Using position and speed sensors in motor control theory, though effective, causes performance degradation and imposes extra cost [5]. Besides, sensors are not durable, and a faulty read on the sensor will lead to a total loss of motor control [3]. It is demanded that the control system must be stable and robust irrespective of such scenarios. To this end, a sensorless approach has been given due attention both in the academia and the industry. The two majorly applied sensorless control methods of IPMSM are the model-based and high-frequency signal injection methods. The model-based approach is suitable for the medium and high-speed application, while the high-frequency signal injection method is useful for the low-speed range [6]. The model-based sensorless control strategy usually depends on the estimation of the back electromotive force (EMF) [5]–[17]. Unlike surface-mounted PMSM, the extended back EMF of IPMSM depends on both rotor speed and state current [5]. Such an effect is a problem in a high load system, for example, in the traction application.

The associate editor coordinating the review of this manuscript and approving it for publication was Gaolin Wang.

Consequently, developing a robust sensorless control strategy is an open research dimension.

Sliding mode (SM)-based control is a robust control algorithm towards the external load and parameter variation. Hence, sliding mode observer (SMO)-based sensorless control has been reported for the induction motor [18]–[20], linear induction motor [21], [22], and permanent magnet linear synchronous motors [23], [24]. Similarly, a super-twisted SMO (STA-SMO) [8], [10] and [16], SMO with sigmoid function [13], an adaptive notch filter-based SMO [24], adaptive linear neural (ADALINE) network-based SMO [7], and adaptive line enhancer (ALE)-based SMO [14] has been used for IPMSM. A model referenced adaptive system (MRAS)-based sensorless control [26], a feedforward control with MRAS-based parameter estimation [27], a linear back EMF observer combined with a hijacker algorithm [9], and a linear moving horizon with luenberger observer state feedback [28] has been applied for sensorless control of IPMSM for different applications. A flux-based model for sensorless control of IPMSM has been reported in [29]-[32], where the low-speed application is achieved. An adaptive nonlinear observer for speed estimation has been reported in [33]. A linearized model of IPMSM has been used to assure system stability and speed adaptation. The author provides the advantage of using nonlinear adaptive observers for sensorless applications. However, linearization only assures the stability of a given system around a specific operating point. A nonlinear approach of gradient descent flux observer with initial rotor position identification is presented in [34].

A disturbance observer-based sensorless control of IPMSM considering the back EMF as an external disturbance is shown in [12], where a zero rate of change of back EMF is assumed. A linear state observer with a zero rate of change of back EMF usually limits the dynamic performance of the system [15]. An unknown input observer-based sensorless control of IPMSM by manipulating the IPMSM mathematical model to resemble as a surface-mounted PMSM is presented in [35]. A similar model to [35] has been used in [36] to estimate the stator flux. A complex disturbance observer is applied for stator flux estimation. This paper presents a simple disturbance observer-based sensorless control of IPMSM using an extended sliding mode disturbance observer (ESMDO). It combines the advantage of extended disturbance observer, and sliding mode towards parameter variation/external load change. The ESMDO is used to estimate the disturbance resulted from parameter variation, frame transformation, and unmodelled dynamics instead of the back EMF as in the conventional SMO-based approach. The approach has been reported in [37] for PMSM parameter identification, where the authors extended the work of [38]. In [38], ESMDO is designed to enhance the performance of the speed controller for IPMSM. The comparative analysis of conventional sliding mode control (SMC) and SMC-ESMDO shows that the latter has a better disturbance rejection quality. Motivated by [37] and [38], in this paper, the ESMDO is extended for current estimation. The effect of parameter variation and frame transformation is considered as a lumped disturbance, and the ESMDO is designed for the sensorless application. Observer stability is guaranteed by using the Lyapunov stability theory. It has been demonstrated that the proposed speed sensorless control method behaves as a low pass filter at the sliding surface, and can effectively suppress the high-frequency disturbances. A sudden change in load and reference speed may result in system instability. Increasing the sliding mode gain usually improves the system stability at the cost of chattering. Consequently, a PI-based feedforward speed compensation algorithm is designed considering the d-axis disturbance. The effectiveness of the proposed method is validated using extensive simulation and hardware-in-the-loop (HIL) test.

The rest of the paper is organized as follows. Section II explains the machine model and the ESMDO. The design procedure of the ESMDO and its implementation for IPMSM current estimation are introduced. The stability analysis of the ESMDO is explained in section III. The stability requirement and controller gain selection procedure is provided. The characteristic of ESMDO at the sliding surface is given, and the necessary condition for stability is presented. The need for a PI feedforward compensation algorithm and design procedure is explained in section IV. Simulation-based validation of the proposed method is explained in section V while section VI explains the HIL test considering different operational conditions. A comparative analysis with the conventional SMO-based sensorless control is given. The final section provides the concluding remark of this paper.

II. IPMSM MACHINE MODEL AND THE ESMDO

IPMSM can be represented in the different mathematical models depending on the reference frames selected or the approach used for sensorless implementation. In this paper, a rotating frame representation is applied. IPMSM in rotating reference frame is represented as [39], [40]:

$$\dot{\lambda}_{dq} = v_{dq} - R_s I_{dq} \pm \omega \lambda_{qd} \tag{1}$$

where λ_{dq} is the dq-axis flux, I_{dq} is the dq-axis current, v_{dq} is the dq-axis voltage, R_s is the motor resistance, and ω is electrical speed. The dq-axis flux is defined as follows:

$$\lambda_{dq} = \begin{bmatrix} L_d I_d + \phi_m \\ L_q i_q \end{bmatrix} \tag{2}$$

L_d is d-axis inductance, L_q is q-axis inductance, and ϕ_m is permanent magnet flux.

To implement the ESMDO-based approach, it is necessary that the following assumption holds.

Assumption I

- *Frame transformation and parameter variation introduces an error*
- *The rate of change of the contributed error is bounded*

The coordinate transformation is formulated as:

$$\begin{bmatrix} \hat{d} \\ \hat{q} \end{bmatrix} = \begin{bmatrix} \cos(\theta_r + \theta_e) & \sin(\theta_r + \theta_e) \\ -\sin(\theta_r + \theta_e) & \cos(\theta_r + \theta_e) \end{bmatrix} \begin{bmatrix} \alpha \\ \beta \end{bmatrix} \tag{3}$$

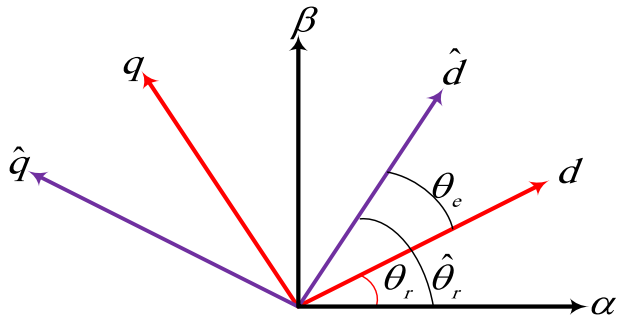

FIGURE 1. Coordinate transformation.

where θ_r is the actual electrical position and θ_e is the position error. The relationship between the approximated and actual frame can be simplified using a reasonable assumption of relatively small angle error (θ_e). Hence, the approximated relationship between the estimated and the actual frame is:

$$\begin{bmatrix} d \\ q \end{bmatrix} = \begin{bmatrix} d' \cos\theta_e - q' \sin(\theta_e) \\ q' \cos\theta_e + d' \sin(\theta_e) \end{bmatrix} \approx \begin{bmatrix} d' + \delta_d \\ q' + \delta_q \end{bmatrix} \tag{4}$$

This can be propagated to the machine model, and the extra-component can be considered as an error or a lumped disturbance. The machine model in the approximated rotating frame is then formulated as:

$$\begin{aligned} L_d \frac{di'_d}{dt} &= v'_d - Ri'_d + L_q \omega_r i'_q + r_d(t), \\ r_d(t) &= \omega_r \phi_f \sin(\theta_e) - L_d \frac{d\delta i'_d}{dt} - \delta v'_d + R\delta i'_d \\ &\quad + L_q \omega_r \delta i'_q + T_q(t) \\ L_q \frac{di'_q}{dt} &= v'_q - Ri'_q - \omega_r \left[L_d i'_d + \varphi_f \right] + r_q(t), \\ r_q(t) &= -L_q \frac{d\delta i'_q}{dt} - \delta v'_q + R\delta i'_q - \omega_r \left[L_d \delta i'_d \right] + T_d(t) \end{aligned} \tag{5}$$

where δ shows a variation due to transformation, T_{dq} is a disturbance resulted from parameter variation and unmodelled dynamics. When the error is compensated properly, then the actual current tracking is possible.

A. THE ESMDO DESIGN APPROACH

This section introduces a step-by-step design procedure for the ESMDO. Suppose the system is defined as:

$$\begin{aligned} \dot{x} &= f(x) + h(x)u + d \\ y &= g(x) \end{aligned} \tag{6}$$

where x is the state variable and $f(x)$, $g(x)$ and $h(x)$ is a function of the state variable with known parameters, d is a disturbance due to unmodelled dynamics, parameter variation, and external disturbance, and y is an output of the system.

Designing a controller without considering the unknown external disturbance will degrade the controller performance and may lead to system instability. However, the disturbance rejection quality of the controller can be improved by integrating the controller with a specific disturbance estimation algorithm. Various disturbance estimation methods have been reported in the literature for different applications, including motor drive systems [41]. In this regard, ESMDO is designed for external disturbance estimation to improve SMC-based speed control of the IPMSM in [37]. A better disturbance rejection quality is achieved using the SMC-ESMDO approach in comparison to the conventional SMC speed controller.

The ESMDO design procedure starts with the estimation of the state variables as follows:

$$\begin{aligned} \dot{\hat{x}} &= f(\hat{x}) + h(\hat{x})u + \hat{d} + u_{smo} \\ \dot{\hat{d}} &= g u_{smo} \end{aligned} \tag{7}$$

where $\hat{d}$ is the estimated disturbance, g is the sliding mode gain, u_{smo} is the switching signal designed as:

$$u_{smo} = \xi sgn(x - \hat{x}) \tag{8}$$

The state estimation error is the difference between (6) and (7).

$$\dot{\tilde{x}} = f(x - \hat{x}) + \left[h(x - \hat{x}) \right] u + d - \hat{d} - u_{smo} \tag{9}$$

Taking the state estimation error as a sliding surface, and s^2 as a Lyapunov function, the stability of the state observer is guaranteed by designing u_{smo} properly [37].

$$\dot{\tilde{x}} = s \left[f(x - \hat{x}) + \left[h(x - \hat{x}) \right] u + \tilde{d} - u_{smo} \right] \tag{10}$$

If the switching signal gain is designed in accordance to the Lyapunov stability requirement, then the sliding surface is reachable. At the sliding where, $s = 0, \dot{s} = 0$, an equivalent control method can be applied.

$$\begin{aligned} \tilde{d} &= u_{smo}, \dot{\tilde{d}} = D - g u_{smo} \leftrightarrow D - g\tilde{d} \\ \tilde{d}(t) &= e^{-gt} \left[C + \int D e^{gt} dt \right] \end{aligned} \tag{11}$$

where C is a constant and D is the maximum rate of change of disturbance. The convergence of the disturbance estimation error highly depends on the parameter g and must be a positive value.

The chattering suppression quality of ESMDO can be understood by considering a certain chattering level Z_0.

$$\tilde{d} = u_{smo} + Z_0, \quad \dot{\tilde{d}} = D - g u_{smo} = D - g\tilde{d} - gZ_0 \tag{12}$$

The transfer function relating the disturbance estimation error to the rate of disturbance and the introduced chattering level is then:

$$F(s) = \frac{\tilde{D}(s)}{D - gZ_0} = \frac{1}{s + g} \tag{13}$$

As per (13), the transfer function $F(s)$ is a low pass filter with a cutoff frequency $fc = g$, and can effectively suppress the high-frequency component. Hence, the ESMDO acquires a good disturbance estimation and chattering suppression quality. Consequently, in this paper, the ESMDO is used to achieve a sensorless control of IPMSM.

B. ESMDO-BASED CURRENT ESTIMATION FOR IPMSM

ESMDO-based disturbance observer under the validation of "*Assumption I*" is designed to circumvent the impact of frame transformation and parameter variation. The ESMDO for current estimation can be designed as:

$$\begin{aligned} L_d\frac{d\hat{i}_d}{dt} &= v_d - R_s\hat{i}_d + \hat{x}_2 + \hat{r}_d(t) + \lambda_d\ \mathrm{sgn}(e_d), \hat{x}_2 = L_q\hat{\omega}_r i_q \\ \dot{\hat{r}}_d(t) &= K_d\ \mathrm{sgn}(e_d) \\ L_q\frac{d\hat{i}_q}{dt} &= v_q - R_s\hat{i}_q - \hat{x}_3 + \hat{r}_q(t) + \lambda_q\ \mathrm{sgn}(e_q), \\ \hat{x}_3 &= \hat{\omega}_r\left[L_d i_d + \varphi_f\right] \\ \dot{\hat{r}}_q(t) &= K_d\mathrm{sgn}(e_q) \end{aligned} \tag{14}$$

Subtracting (14) form (5), the error dynamics is:

$$\begin{aligned} L_d\frac{de_d}{dt} &= -\mathrm{Re}_d + x_2 - \hat{x}_2 + r_d(t) - \hat{r}_d(t) - \gamma_d\ \mathrm{sgn}(e_d) \\ \dot{e}_{r_d}(t) &= d_d(t) - k_d\ \mathrm{sgn}(e_d) \\ L_q\frac{de_q}{dt} &= -\mathrm{Re}_q - x_3 + \hat{x}_3 + r_q(t) - \hat{r}_q(t) - \gamma_q\ \mathrm{sgn}(e_q) \\ \dot{e}_{r_q}(t) &= d_q(t) - k_q\ \mathrm{sgn}(e_q) \end{aligned} \tag{15}$$

where d_{dq} is the rate of change of the lumped disturbance r_{dq}. Under proper selection of the observer gain, efficient current estimation is achievable. The observer gains must be selected following the stability requirement.

III. STABILITY ANALYSIS AND SPEED ESTIMATION

The designed current observer must be stable irrespective of the operational conditions. A Lyapunov stability theory is applied to assure the stability of the proposed current observer.

$$\begin{aligned} V &= L_d\,(e_d)^2 + L_q\left(e_q\right)^2 + (e_\omega)^2 \\ \dot{V} &= e_d\left[-\mathrm{Re}_d + x_2 - \hat{x}_2 + e_{r_d}(t) - \gamma_d\ \mathrm{sgn}(e_d)\right] \\ &\quad + e_q\left[-\mathrm{Re}_q - x_3 + \hat{x}_3 + e_{r_q}(t) - \gamma_q\ \mathrm{sgn}(e_q)\right] + e_\omega\,(\dot{e}_\omega) \end{aligned} \tag{16}$$

By rearranging (16), the derivative of the Lyapunov function will be:

$$\begin{aligned} \dot{V} &= -Re_d^2 - Re_q^2 + e_\omega\left[L_q e_d i_q - L_d e_q i_d - e_q\phi + \gamma\dot{e}_\omega\right] \\ &\quad + e_d\left[e_{r_d}(t) - \gamma_d\ \mathrm{sgn}(e_d)\right] + e_q\left[e_{r_q}(t) - \gamma_q\ \mathrm{sgn}(e_q)\right] \end{aligned} \tag{17}$$

Under the assumption of a higher mechanical time constant compared to the electrical one, $\dot{\omega}_r = 0$, the electrical speed can be estimated as:

$$\hat{\omega}_r = K_s\int\left[e_d\varphi_q - e_q\varphi_d\right]dt \tag{18}$$

Direct integration of the electrical speed will give us an electrical position. However, the reachability of the sliding surface requires the appropriate selection of the sliding gains. The necessary and sufficient conditions that guarantee the stability of the proposed ESMDO is to select γ_{dq} as (18).

$$\begin{cases} e_d\left[e_{r_d}(t) - \gamma_d\right] \le 0, e_d > 0 \\ e_d\left[e_{r_d}(t) + \gamma_d\right] \le 0, e_d < 0 \end{cases} \leftrightarrow \gamma_d > \left\|e_{r_d}(t)\right\|$$

$$\begin{cases} e_q\left[e_{r_q}(t) - \gamma_q\right] \le 0, e_q > 0 \\ e_d\left[e_{r_q}(t) + \gamma_q\right] \le 0, e_q < 0 \end{cases} \leftrightarrow \gamma_q > \left\|e_{r_q}(t)\right\| \tag{19}$$

At the sliding surface $s_d = \dot{s}_d = 0, s_q = \dot{s}_q = 0$, an equivalent control method will give us an insight into the nature of the disturbance estimation. From the very nature of ESMDO, it is understood that the disturbance estimation gain determines the convergence rate of the disturbance estimation error towards the equilibrium point.

$$\begin{aligned} 0 &= L_q i_q(\omega - \hat{\omega}) + \tilde{r}_d(t) - \gamma_d\ \mathrm{sgn}(e_d) \\ \dot{e}_{r_d}(t) &= d_d(t) - k_d\ \mathrm{sgn}(e_d) \\ 0 &= -(L_d i_d + \varphi_f)(\omega - \hat{\omega}) + \tilde{r}_q(t) - \gamma_q\ \mathrm{sgn}(e_q) \\ \dot{e}_{r_q}(t) &= d_q(t) - k_q\ \mathrm{sgn}(e_q) \end{aligned} \tag{20}$$

If we have good tracking, then speed estimation error can be assumed negligible and will not be considered in disturbance estimation error analysis.

$$\begin{aligned} \frac{\tilde{r}_d(t)}{\gamma_d} &= \mathrm{sgn}(e_d) \leftrightarrow \dot{e}_{r_d}(t) = d_d(t) - k_d\frac{\tilde{r}_d(t)}{\gamma_d} \\ \frac{\tilde{r}_q(t)}{\gamma_q} &= \mathrm{sgn}(e_q) \leftrightarrow \dot{e}_{r_q}(t) = d_q(t) - k_q\frac{\tilde{r}_q(t)}{\gamma_q} \end{aligned} \tag{21}$$

Laplace transforming (21) yields:

$$\begin{aligned} \frac{e_{r_d}(s)}{d_d(s)} &= \frac{1}{[s + a_d]}, \frac{e_{r_q}(s)}{d_q(s)} = \frac{1}{[s + a_q]}, \\ a_d &= k_d/\gamma_d, a_q = k_q/\gamma_q \end{aligned} \tag{22}$$

where $f_c = \alpha_{dq}$ is the cutoff frequency of an inherent low pass filter. The convergence of disturbance estimation error depends on α_{dq}. Generally, the ESMDO-based sensorless control method highly depends on the sliding parameters, and these parameters must be selected as per the stability requirement. The use of a crispy sign function usually experiences an extreme chattering, and in this paper, a tanh function is used instead.

IV. A COMPENSATION METHOD

The disturbance and its rate are unknown in the real systems, and failure to compensate for the associated impact may result in system instability. The system stability can be assured using very large ESMDO gains that further increases the chattering level. In this regard, we can design a compensator using the induced disturbances during the current estimation. From (5), it is understood that under the assumption of constant motor parameters and efficient position estimation, the dq-disturbances are expected to be negligible. This situation can be used to design a compensator. Both the d and q-axis disturbance has a similar characteristic and can be used for the compensator design. In this paper, a PI compensator is designed using the d-axis disturbance. A low-pass filter is added to smoothen the estimated speed that may exhibit a chattering level due to the introduction of the compensator. It must be understood that there may exist a certain level of disturbance as a speed estimation error cannot be avoided totally. The proposed compensator based sensorless control

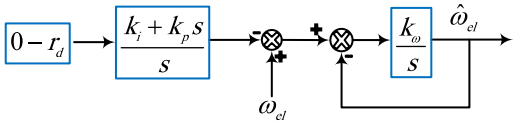

FIGURE 2. Feedforward speed compensation technique.

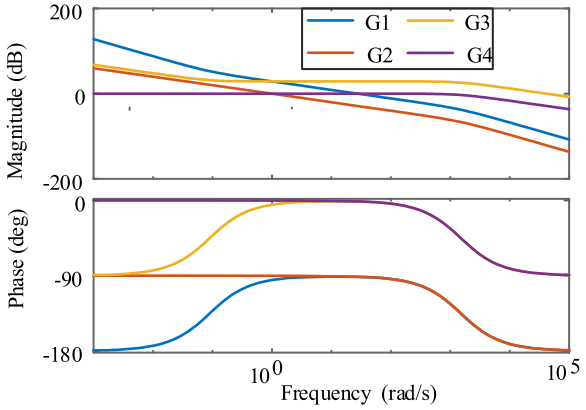

FIGURE 3. Frequency domain analysis of the transfer functions for ki = 2.5, kp = 28, kw = 1500.

is shown in Figure 2. Frequency-domain analysis of the compensator will give us a glimpse of understanding about the effect of d-axis disturbance on the speed and position estimation. The transfer function relating the speed and position component to the d-axis disturbance is presented in (23) and (24).

$$G_1 = \frac{\hat{\theta}_{el}}{r_d} = \frac{k_w\left[k_i + sk_p\right]}{s^2(s + k_w)}, \quad G_2 = \frac{\hat{\theta}_{el}}{\omega_{el}} = \frac{k_w}{s(s + k_w)} \tag{23}$$

$$G_3 = \frac{\hat{\omega}_{el}}{\omega_{el}} = \frac{k_\omega}{s + k_\omega}, \quad G_4 = \frac{\hat{\omega}_{el}}{r_d} = \frac{k_\omega\left[k_i + sk_p\right]}{s\left[s + k_\omega\right]} \tag{24}$$

The bode plot of the transfer functions (23) and (24) are depicted in Figure 3. At the lower frequency range, the effect of disturbance on speed estimation is damped with a rate of −20 dB while there is no damping effect for medium frequency range, and the disturbance appears in the estimated speed. Hence, speed compensation in this range is enhanced by the designed compensator. The effect of disturbance above the low-pass filter cutoff frequency is also damped at a rate of −20 dB. The low-pass filter cutoff frequency must be selected in such a way that the operational condition is satisfied. It is identified that the low-pass filter cutoff frequency must be greater than the rated speed of the motor.

The effect of disturbance on position estimation can be easily understood from Figure 3. At the low-frequency range, the effect of disturbance is damped at a rate of −40 dB, and a −20 dB damping rate is observed for the frequency range lower than the low-pass filter cutoff frequency. Above the low-pass filter cutoff frequency, the impact of d-axis disturbance on the electrical position is damped at a rate of −40 dB. Consequently, the effect of disturbance is damped in the operating frequency range.

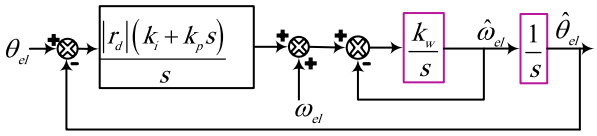

FIGURE 4. Closed-loop representation of the proposed method.

TABLE 1. PMSM properties.

Parameter	Value	Parameter	Value
stator resistance(Ω)	0.0459	rated/peak power(kW)	190/305
Ld (mH)	1.58	rated/peak voltage (V)	926/1170
Lq (mH)	3.96	rated/peak current (A)	138/200
Flux (Wb)	0.6838	rated frequency (Hz)	120
pole-pairs	4	rated dc voltage (V)	1500

Hence, the designed PI compensator improves the performance of the speed estimation algorithm based on the d-axis disturbance. From the model (5), it is understood that the d-axis disturbance may be represented as a function of electrical position error under the assumption of constant motor parameters. This condition is used to design the PI speed compensator gains. The effect of the d-axis disturbance is damped properly for the position, and speed is compensated well in the operating range.

The compensator gains are selected by considering constant motor parameters, from (5), the d-axis disturbance may be represented as a function of position error.

$$r_d \approx |r_d|\left(\theta_{el} - \hat{\theta}_{el}\right) \tag{25}$$

The closed-loop transfer function can be drawn by using this assumption. Hence, the closed-loop representation of the proposed approach is then depicted in Figure 4.

The closed-loop transfer function is then obtained as:

$$\hat{\theta}_{el} = \frac{|r_d|\,k_w\left[k_i + sk_p\right]}{s^3 + k_w s^2 + |r_d|\,k_w\left[k_i + sk_p\right]}\theta_{el} + \frac{sk_w}{s^3 + k_w s^2 + |r_d|\,k_w\left[k_i + sk_p\right]}\omega_{el} \tag{26}$$

The stability of the closed-loop system depends on the location of the roots of the characteristic equation. Routh's-Hurwitz stability criterion can be used to ensure closed-loop stability. Hence, $k_p k_\omega \geq k_i$ and all $k's$ must be greater than zero to ensure the stability of the closed-loop system. It is identified that the value of k_w should be greater than the rated speed of the motor to ensure the smooth operation of the proposed method.

V. SIMULATION RESULT

The performance of the proposed speed sensorless control method is validated using an extensive simulation considering different operational conditions. The motor parameters are shown in Table 1. A PI controller with ant-winding nature is applied for both speed and current control.

The model-based approaches are efficient in medium to high-speed operating ranges. Consequently, the performance

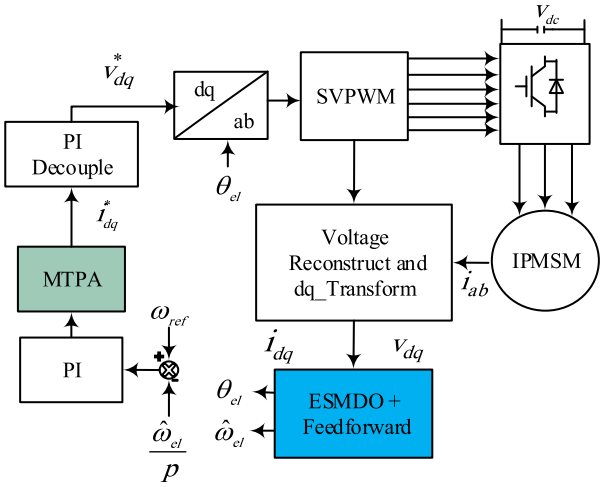

FIGURE 5. Proposed ESMDO based sensorless control of IPMSM.

TABLE 2. Controller parameters.

Controller	P	I	
Speed Controller	9	55	
Current Controller	5	155	
ESTIMATION PARAMETERS			
K_d , K_q	1900	γ_d, γ_q	4900
K_i	2.5	K_p	28
K_w	1500	K_s	1240

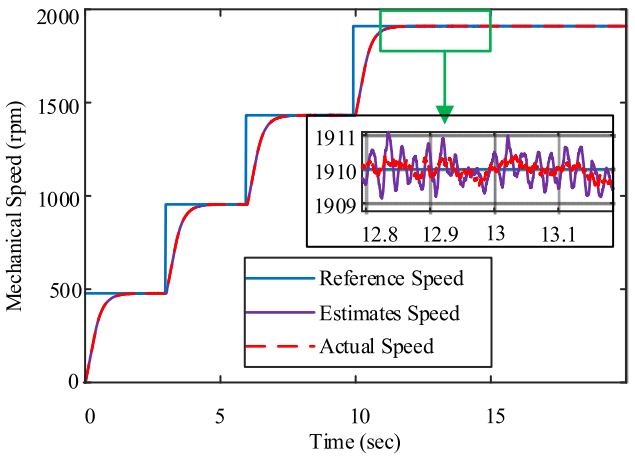

FIGURE 6. Speed estimation under a speed change.

of the proposed sensorless control is tested in this range. The reference currents are obtained from a maximum torque per ampere (MTPA) principle.

The overall speed sensorless control scheme is shown in Figure 5. The simulation parameters are shown in Table 2.

A. DYNAMIC PERFORMANCE FOR A STEP SPEED AND A CONSTANT LOAD

The mechanical reference speed is varied from 50 rad/sec to 200 rad/sec with a step of 50 rad/sec under a constant load of 800 Nm. The simulation result for such an operating

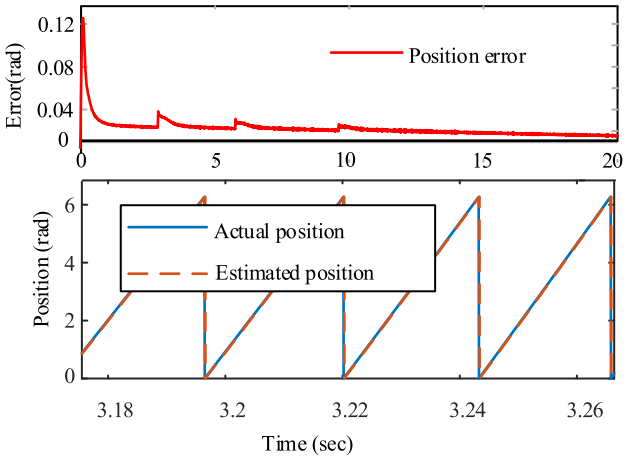

FIGURE 7. Position estimation under a speed change.

TABLE 3. External load variation.

Load (Nm)	Mechanical Speed (rad/sec)	Application time (sec)
0		0-10
400		10-15
800	200	15-20
400		20-25
0		>25

condition is shown in Figure 6 and Figure 7. Figure 6 constitutes the reference, actual, and the estimated speed. Figure 7 shows the electrical position that includes the actual position, estimated position, and the estimation error. From the simulation result, it is understood that the proposed control method has a good speed estimation performance. Similarly, Figure 7 prevails that the position estimation error is very small, where the proposed control method is robust towards a step-change in mechanical speed. A further controller improvement can be achieved through a reasonable tuning of the PI controller gains or by introducing a more robust nonlinear control method.

B. DYNAMIC PERFORMANCE UNDER LOAD CHANGE

The controller designed for railway applications must be robust towards an inevitable external load variation. Consequently, the proposed speed sensorless control method is evaluated considering an operational condition of Table 3.

The dynamic performance of the proposed sensorless control method under such an operational condition is shown in Figure 8. It can be understood that the method achieves a good speed estimation accuracy and control stability under external load variation. Similarly, the electrical position is shown in Figure 9. Some position error transient is experienced during an external load change. However, the estimation error converges to zero in the steady-state, and the error is very small.

In general, the proposed speed sensorless control method is robust towards external load variation.

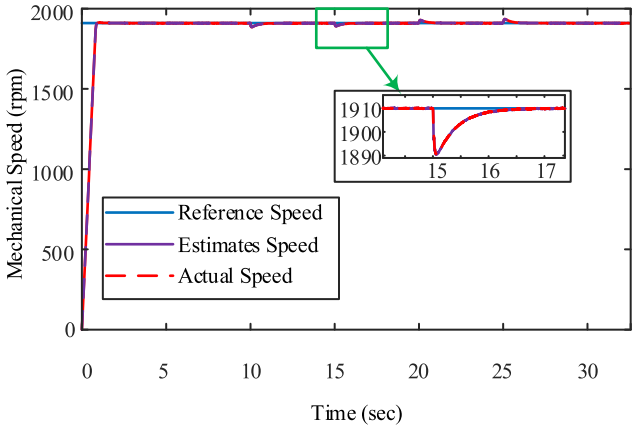

FIGURE 8. Speed estimation during load variation.

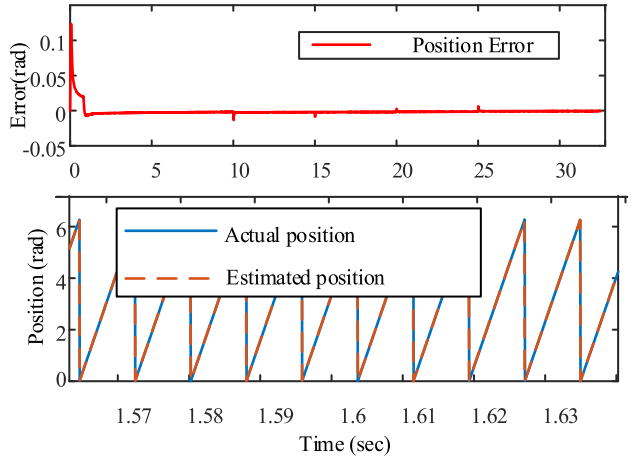

FIGURE 9. Position estimation during load variation.

TABLE 4. Ramp reference speed.

Load (Nm)	Mechanical Speed (rad/sec)	Application time (sec)
800	100	0-5
	20*(t-5)+100	5-10
	200	10-20
	-20*(t-10)+200	20-30
	100	>30

C. DYNAMIC PERFORMANCE FOR RAMP SPEED CHANGE UNDER A CONSTANT LOAD

In the metro system, the train passes through acceleration, deceleration, coasting, and uniform motion. Hence, the proposed sensorless control method must be evaluated for such operational dynamics. The detailed operational condition is as per Table 4.

The speed estimation is shown in Figure 10. The result prevails that the proposed speed sensorless control method achieves a good speed estimation quality. Figure 11 shows the electrical position and estimation error, which is very small. Hence, the proposed ESMDO-based sensorless control is robust and efficient during acceleration/deceleration.

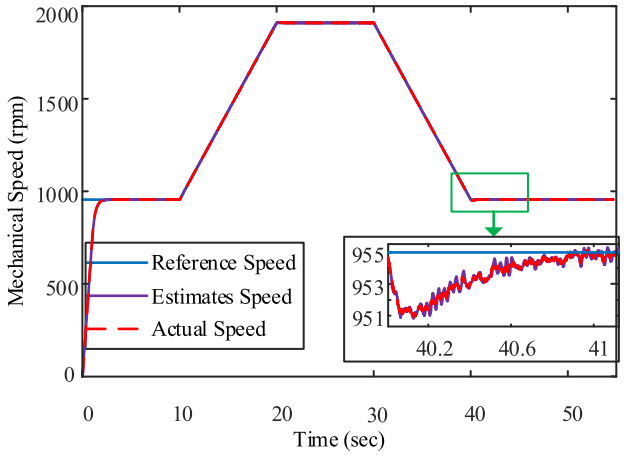

FIGURE 10. Speed estimation under ramp speed reference.

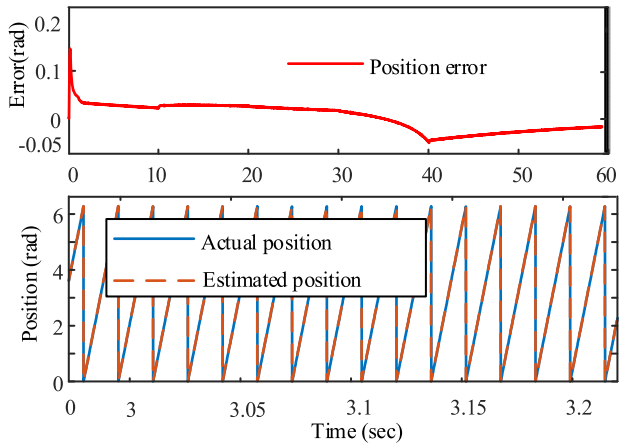

FIGURE 11. Position estimation under ramp speed.

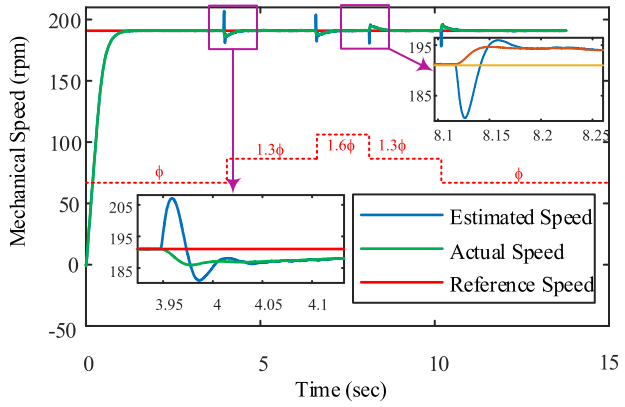

FIGURE 12. Speed estimation under permanent magnet flux variation.

D. DYNAMIC PERFORMANCE UNDER PARAMETER VARIATION

The performance of the proposed sensorless control method is tested for permanent magnet flux variation at 10% of the rated speed. The applied load torque is 800 Nm. The simulation result is depicted in Figure 12. Although the parameter variation causes a certain speed transient, the proposed speed sensorless control method has a good speed

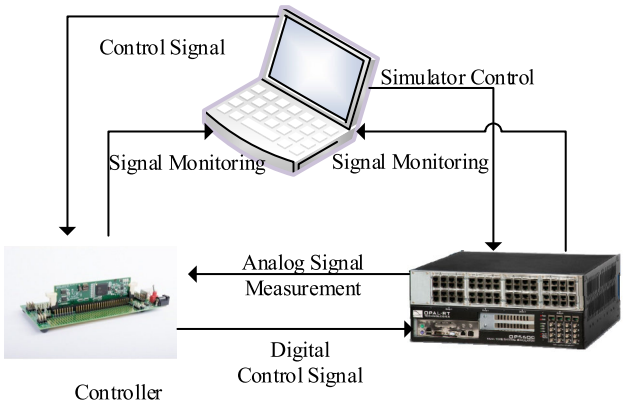

FIGURE 13. The HIL test configuration.

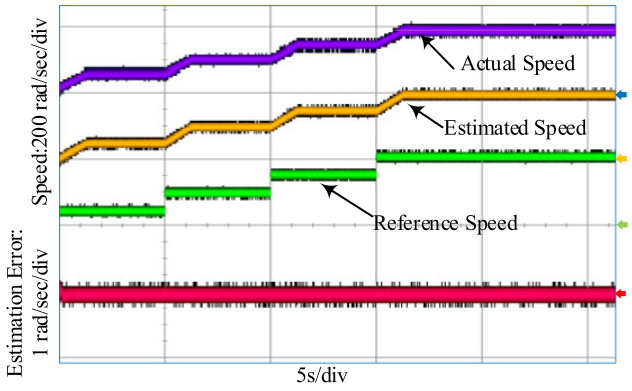

FIGURE 14. HIL result for step reference speed change.

estimation quality. The lowest effective speed subjected to parameter variation is 10% of the rated speed. However, an improvement of the lowest effective speed is possible by reasonably tuning the controller parameters.

VI. THE HIL TEST

The proposed speed sensorless control method is further validated by the HIL test using the TMS320F28335 control unit in the OP5600 real-time simulation environment. A delay compensation presented in [42] is adopted. Sampling time of 70e-6 sec and a switching frequency of 1.5 kHz is used. Figure 13 shows the overall HIL test configuration. A similar operational condition to that of the simulation is used.

A HIL test result for step reference speed change under a constant load of 800 Nm is shown in Figure 14. The reference mechanical speed is varied from 50 rad/sec to 200 rad/sec with a step of 50 rad/sec. It can be seen that the proposed speed sensorless control method exhibits a good speed estimation quality. The result is coherent with the simulation result depicted in Figure 6.

The proposed sensorless approach must be robust towards external load variation, which is common in the metro system. In this regard, the HIL test is performed under the operating condition stated in Table 3. The result is captured in Figure 15. The speed estimation error is very small, and the effect of external load variation on speed estimation is not observed.

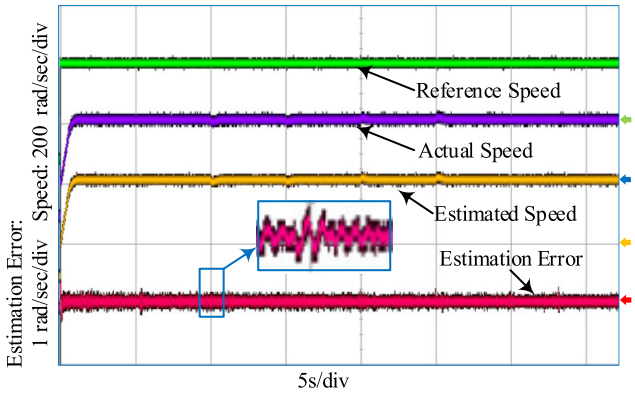

FIGURE 15. HIL test result for speed estimation under external load change.

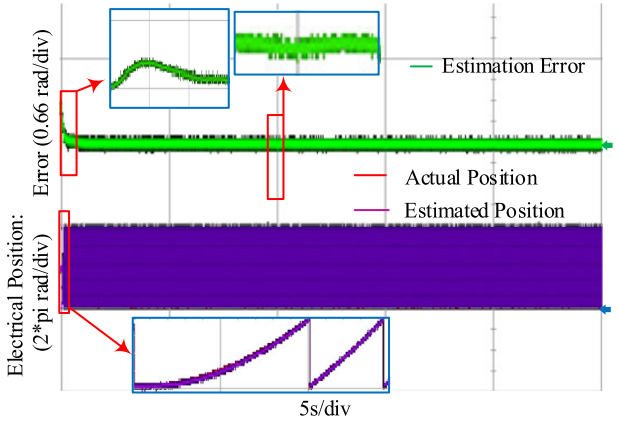

FIGURE 16. HIL test result for position estimation under external load change.

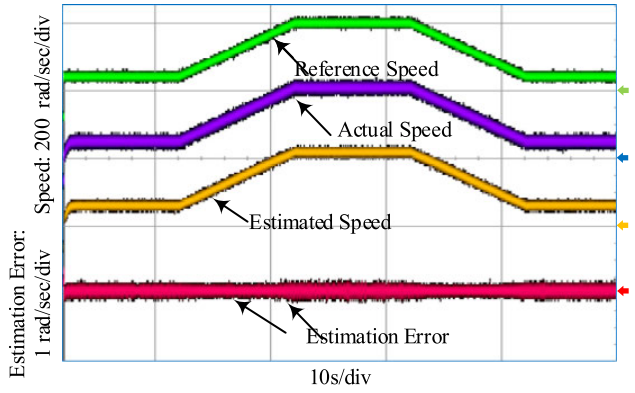

FIGURE 17. HIL test under ramp speed change.

The electrical position estimation is shown in Figure 16. The effect of external load variation on position estimation is negligible as the position error due to the external load change is very small. The proposed speed sensorless control method is robust towards external load variation. The experimental result is coherent with the simulation result sown in Figure 8 and Figure 9. Hence, disturbance rejection quality of the proposed ESMDO is verified.

Similarly, the HIL test of ramp speed change under a constant load of 800 Nm is conducted, and the result is shown in Figure 17. From the result, it is understood that

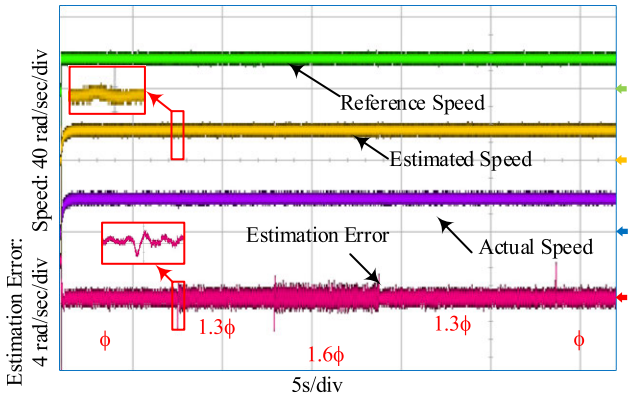

FIGURE 18. HIL test speed estimation performance under permanent magnet flux change.

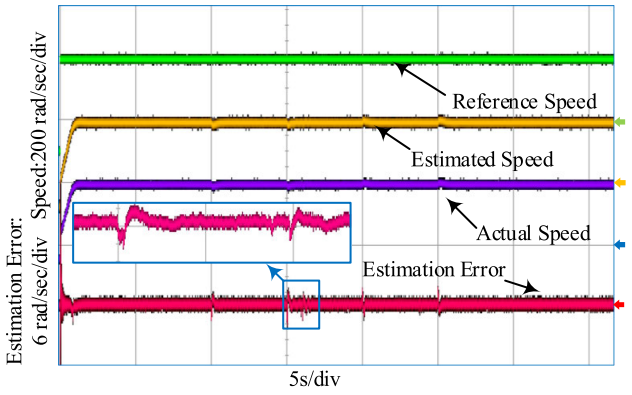

FIGURE 19. HIL test speed estimation performance of SMO-based approach for variable load.

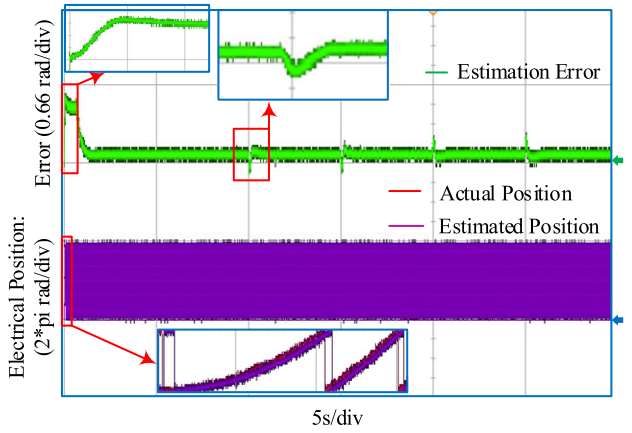

FIGURE 20. HIL test position estimation performance of SMO-based SMO based approach for variable load.

the proposed speed sensorless control method properly estimates the actual speed of the motor. The estimation error is very small, which leads to stable motor operation. The experimental result is coherent with the simulation result depicted in Figure 10. Hence, the proposed ESMDO-based sensorless control of IPMSM is efficient towards a ramp reference speed.

Motor parameter variation is common in the real application, and the proposed speed sensorless control is tested for a permanent magnet flux change. The system operates at a mechanical speed of 20 rad/s and 800 Nm external load. The lowest allowable speed with the mentioned controller parameter is 10% of the rated speed. The permanent magnet flux is varied from ϕ_m to 1.3 ϕ_m to 1.6 ϕ_m and back to 1.3 ϕ_m to ϕ_m. The HIL test result is depicted in Figure 18. From the result, it can be observed that the speed estimation error is very small, and the stability of the system is not disturbed due to a step-change in the permanent magnet flux. Hence, a stable operation is guaranteed even under permanent magnet flux change.

In general, the robustness of the proposed speed sensorless control method towards external load variation, speed reference change, and motor parameter variation is validated using simulation and HIL tests. The proposed speed sensorless approach achieves an efficient sensorless control of IPMSM as low as 10% of the rated speed subjected to motor parameter variation.

A comparative study of the proposed speed sensorless control method with other sensorless control methods will allow us to understand the performance improvement of the proposed method. In this regard, a comparative analysis with the conventional SMO-based sensorless control method is conducted.

The speed estimation performance of the SMO-based sensorless method at a speed of 200 rad/sec and external load variation of Table 3 is shown in Figure 19. It can be observed that the SMO-based speed sensorless control method effectively captures the reference speed under external load variation. The load change resulted in a speed estimation transient, whereas the proposed method doesn't have a speed estimation error transient (Figure 15). Similarly, the position and estimation error of SMO is shown in Figure 20. In comparison to the ESMDO-based result shown in Figure 16, the position estimation error is higher, and transient error is observed during an external load change. Such conditions may result in low sensorless control performance.

The performance comparison prevails that the conventional SMO-based sensorless control method has a higher speed estimation and position error during load change that may affect controller stability and robustness. The proposed speed sensorless control method, on the other hand, provides a better speed estimation accuracy and disturbance rejection quality.

In general, the proposed speed sensorless control method can be considered as a sensorless control solution for the metro application that requires a low switching frequency.

VII. CONCLUSION

In this paper, a nonlinear speed adaptation mechanism using an extending sliding mode disturbance observer (ESMDO) is presented. The system formulation considers frame transformation effect and parameter variation as a lumped disturbance. The lumped disturbances are then estimated by using

the ESMDO. A step-by-step machine modeling for ESMDO implementation and ESMDO design procedure is presented.

The stability of the proposed speed sensorless control method is guaranteed using a Lyapunov stability theory. A PI compensator is introduced to ensure smooth reference tracking for different operating conditions. The proposed method has an internal low pass filter that improves its chattering elimination quality compared to the conventional SMO-based sensorless control method.

The proposed speed sensorless control method is validated using extensive simulation and a hardware-in-the-loop (HIL) test with the TMS320F28335 control unit in the real-time environment. The result confirms the theoretical analysis.

The metro system requires a low switching frequency and the switching frequency of the proposed sensorless control is not too high. Consequently, the proposed sensorless control method can be considered as a solution for the metro application for the medium and high-speed range.

REFERENCES

[1] C. Calleja, López-de-Heredia, H. Gaztañaga, T. Nieva, and L. Aldasoro, "Validation of a modified direct-self-control strategy for PMSM in railway-traction applications," *IEEE Trans. Ind. Electron.*, vol. 63, no. 8, pp. 5143–5155, Aug. 2016.

[2] A. Nasiri, "Full digital current control of permanent magnet synchronous motors for vehicular applications," *IEEE Trans. Veh. Technol.*, vol. 56, no. 4, pp. 1531–1537, Jul. 2007.

[3] M.-S. Lim, S.-H. Chai, and J.-P. Hong, "Design of saliency-based sensorless-controlled IPMSM with concentrated winding for EV traction," *IEEE Trans. Magn.*, vol. 52, no. 3, Mar. 2016, Art. no. 8200504.

[4] A. Shinohara, Y. Inoue, S. Morimoto, and M. Sanada, "Maximum torque per ampere control in stator flux linkage synchronous frame for DTC-based PMSM drives without using q-axis inductance," *IEEE Trans. Ind. Appl.*, vol. 53, no. 4, pp. 3663–3671, Jul/Aug. 2017.

[5] Y. Zhao, W. Qiao, and L. Wu, "An adaptive quasi-sliding-mode rotor position observer-based sensorless control for interior permanent magnet synchronous machines," *IEEE Trans. Power Electron.*, vol. 28, no. 12, pp. 5618–5629, Dec. 2013.

[6] S. Bolognani, S. Calligaro, and R. Petrella, "Design issues and estimation errors analysis of back-EMF-based position and speed observer for SPM synchronous motors," *IEEE J. Emerg. Sel. Topics Power Electron.*, vol. 2, no. 2, pp. 159–170, Jun. 2014.

[7] G. Zhang, G. Wang, D. Xu, and N. Zhao, "ADALINE-network-based PLL for position sensorless interior permanent magnet synchronous motor drives," *IEEE Trans. Power Electron.*, vol. 31, no. 2, pp. 1450–1460, Feb. 2016.

[8] D. Liang, J. Li, R. Qu, and W. Kong, "Adaptive second-order sliding-mode observer for PMSM sensorless control considering VSI nonlinearity," *IEEE Trans. Power Electron.*, vol. 33, no. 10, pp. 8994–9004, Oct. 2018.

[9] P. M. Johnson, K. Bai, and X. Ding, "Back-EMF-based sensorless control using the Hijacker algorithm for full speed range of the motor drive in electrified automobile systems," *IEEE Trans. Transp. Electrific.*, vol. 1, no. 2, pp. 126–137, Aug. 2015.

[10] J. R. Domínguez, A. Navarrete, M. A. Meza, A. G. Loukianov, and J. Cañedo, "Digital sliding-mode sensorless control for surface-mounted PMSM," *IEEE Trans. Ind. Informat.*, vol. 10, no. 1, pp. 137–151, Feb. 2014.

[11] G. Wang, L. Ding, Z. Li, J. Xu, G. Zhang, H. Zhan, R. Ni, and D. Xu, "Enhanced position observer using second-order generalized integrator for sensorless interior permanent magnet synchronous motor drives," *IEEE Trans. Energy Convers.*, vol. 29, no. 2, pp. 486–495, Jun. 2014.

[12] Z. Chen, M. Tomita, S. Doki, and S. Okuma, "An extended electromotive force model for sensorless control of interior permanent-magnet synchronous motors," *IEEE Trans. Ind. Electron.*, vol. 50, no. 2, pp. 288–295, Apr. 2003.

[13] H. Kim, J. Son, and J. Lee, "A high-speed sliding-mode observer for the sensorless speed control of a PMSM," *IEEE Trans. Ind. Electron.*, vol. 58, no. 9, pp. 4069–4077, Sep. 2011.

[14] Y. Zhao, W. Qiao, and L. Wu, "Improved rotor position and speed estimators for sensorless control of interior permanent-magnet synchronous machines," *IEEE J. Emerg. Sel. Topics Power Electron.*, vol. 2, no. 3, pp. 627–639, Sep. 2014.

[15] G. Wang, Z. Li, G. Zhang, Y. Yu, and D. Xu, "Quadrature PLL-based high-order sliding-mode observer for IPMSM sensorless control with online MTPA control strategy," *IEEE Trans. Energy Convers.*, vol. 28, no. 1, pp. 214–224, Mar. 2013.

[16] D. Liang, J. Li, and R. Qu, "Sensorless control of permanent magnet synchronous machine based on second-order sliding-mode observer with online resistance estimation," *IEEE Trans. Ind. Appl.*, vol. 53, no. 4, pp. 3672–3682, Jul./Aug. 2017.

[17] F.-J. Lin, Y.-C. Hung, J.-M. Chen, and C.-M. Yeh, "Sensorless IPMSM drive system using saliency back-EMF-based intelligent torque observer with MTPA control," *IEEE Trans. Ind. Informat.*, vol. 10, no. 2, pp. 1226–1241, May 2014.

[18] L. Zhao, J. Huang, H. Liu, B. Li, and W. Kong, "Second-order sliding-mode observer with online parameter identification for sensorless induction motor drives," *IEEE Trans. Ind. Electron.*, vol. 61, no. 10, pp. 5280–5289, Oct. 2014.

[19] M. Ghanes and G. Zheng, "On sensorless induction motor drives: Sliding-mode observer and output feedback controller," *IEEE Trans. Ind. Electron.*, vol. 56, no. 9, pp. 3404–3413, Sep. 2009.

[20] S. Di Gennaro, J. R. Domínguz, and M. A. Meza, "Sensorless high order sliding mode control of induction motors with core loss," *IEEE Trans. Ind. Electron.*, vol. 61, no. 6, pp. 2678–2689, Jun. 2014.

[21] H. Wang, X. Ge, and Y.-C. Liu, "Second-order sliding-mode MRAS observer-based sensorless vector control of linear induction motor drives for medium-low speed maglev applications," *IEEE Trans. Ind. Electron.*, vol. 65, no. 12, pp. 9938–9952, Dec. 2018.

[22] H. Wang, Y.-C. Liu, and X. Ge, "Sliding-mode observer-based speed-sensorless vector control of linear induction motor with a parallel secondary resistance online identification," *IET Electr. Power Appl.*, vol. 12, no. 8, pp. 1215–1224, Sep. 2018.

[23] C. Yang, T. Ma, Z. Che, and L. Zhou, "An adaptive-gain sliding mode observer for sensorless control of permanent magnet linear synchronous motors," *IEEE Access*, vol. 6, pp. 3469–3478, 2017.

[24] Z. Li, S. Zhou, Y. Xiao, and L. Wang, "Sensorless vector control of permanent magnet synchronous linear motor based on self-adaptive super-twisting sliding mode controller," *IEEE Access*, vol. 7, pp. 44998–45011, 2019.

[25] G. Wang, H. Zhan, G. Zhang, X. Gui, and D. Xu, "Adaptive compensation method of position estimation harmonic error for EMF-based observer in sensorless IPMSM drives," *IEEE Trans. Power Electron.*, vol. 29, no. 6, pp. 3055–3064, Jun. 2014.

[26] Y. Zhu, M. Cheng, W. Hua, and B. Zhang, "Sensorless control strategy of electrical variable transmission machines for wind energy conversion systems," *IEEE Trans. Magn.*, vol. 49, no. 7, pp. 3383–3386, Jul. 2013.

[27] O. C. Kivanc and S. B. Ozturk, "Sensorless PMSM drive based on stator feedforward voltage estimation improved with MRAS multiparameter estimation," *IEEE/ASME Trans. Mechatronics*, vol. 23, no. 3, pp. 1326–1337, Jun. 2018.

[28] A. Andersson and T. Thiringer, "Motion sensorless IPMSM control using linear moving horizon estimation with luenberger observer state feedback," *IEEE Trans. Transport. Electrific.*, vol. 4, no. 2, pp. 464–473, Jun. 2018.

[29] W. Xu, Y. Jiang, C. Mu, and F. Blaabjerg, "Improved nonlinear flux observer-based second-order SOIFO for PMSM sensorless control," *IEEE Trans. Power Electron.*, vol. 34, no. 1, pp. 565–579, Jan. 2019.

[30] Y. Zhao, Z. Zhang, W. Qiao, and L. Wu, "An extended flux model-based rotor position estimator for sensorless control of salient-pole permanent-magnet synchronous machines," *IEEE Trans. Power Electron.*, vol. 30, no. 8, pp. 4412–4422, Aug. 2015.

[31] G. H. B. Foo and M. F. Rahman, "Direct torque control of an IPM-synchronous motor drive at very low speed using a sliding-mode stator flux observer," *IEEE Trans. Power Electron.*, vol. 25, no. 4, pp. 933–942, Apr. 2010.

[32] M. Moradian, J. Soltani, A. Najjar-Khodabakhsh, and G. R. A. Markadeh, "Adaptive torque and flux control of sensorless IPMSM drive in the stator flux field oriented reference frame," *IEEE Trans. Ind. Informat.*, vol. 15, no. 1, pp. 205–212, Jan. 2019.

[33] A. Piippo, M. Hinkkanen, and J. Luomi, "Analysis of an adaptive observer for sensorless control of interior permanent magnet synchronous motors," *IEEE Trans. Ind. Electron.*, vol. 55, no. 2, pp. 570–576, Feb. 2008.
[34] A. Khlaief, M. Bendjedia, M. Boussak, and M. Gossa, "A nonlinear observer for high-performance sensorless speed control of IPMSM drive," *IEEE Trans. Power Electron.*, vol. 27, no. 6, pp. 3028–3040, Jun. 2012.
[35] M. Hasegawa, S. Yoshioka, and K. Matsui, "Position sensorless control of interior permanent magnet synchronous motors using unknown input observer for high-speed drives," *IEEE Trans. Ind. Appl.*, vol. 45, no. 3, pp. 938–946, May 2009.
[36] Y. Park and S.-K. Sul, "Sensorless control method for PMSM based on frequency-adaptive disturbance observer," *IEEE J. Emerg. Sel. Topics Power Electron.*, vol. 2, no. 2, pp. 143–151, Jun. 2014.
[37] X. Zhang and Z. Li, "Sliding-mode observer-based mechanical parameter estimation for permanent magnet synchronous motor," *IEEE Trans. Power Electron.*, vol. 31, no. 8, pp. 5732–5745, Aug. 2016.
[38] X. Zhang, L. Sun, K. Zhao, and L. Sun, "Nonlinear speed control for PMSM system using sliding-mode control and disturbance compensation techniques," *IEEE Trans. Power Electron.*, vol. 28, no. 3, pp. 1358–1365, Mar. 2013.
[39] R. Krishnan, *Electric Motor Drives: Modeling Analysis: Modeling, Analysis, and Control*. Upper Saddle River, NJ, USA: Prentice-Hall, 2001.
[40] P. Pillay and R. Krishnan, "Modeling of permanent magnet motor drives," *IEEE Trans. Ind. Electron.*, vol. IE-35, no. 4, pp. 537–541, Nov. 1988.
[41] J. Yang, W.-H. Chen, S. Li, L. Guo, and Y. Yan, "Disturbance/uncertainty estimation and attenuation techniques in PMSM drives—A survey," *IEEE Trans. Ind. Electron.*, vol. 64, no. 4, pp. 3273–3285, Apr. 2017.
[42] M. Lu, X. Wang, P. C. Loh, F. Blaabjerg, and T. Dragicevic, "Graphical evaluation of time-delay compensation techniques for digitally controlled converters," *IEEE Trans. Power Electron.*, vol. 33, no. 3, pp. 2601–2614, Mar. 2018.

ABEBE TEKLU WOLDEGIORGIS received the B.Sc. degree in electrical engineering from Alemaya University, in 2009, and the M.Sc. degree in electrical engineering for railway systems from the Addis Ababa University, Ethiopia, in 2014. He is currently pursuing the Ph.D. degree in rail transit electrification and information technology with Southwest Jiaotong University, China. He was a Lecturer with Addis Ababa University.

His research interests include system modeling of permanent magnet motors, sensorless control of IPMSM, robust control of IPMSM, applications in the railway systems, and hardware-in-the-loop simulation of traction converter and motor drives.

XINGLAI GE (M'15) received the B.S., M.S., and Ph.D. degrees in electrical engineering from Southwest Jiaotong University, Chengdu, China, in 2001, 2004, and 2010, respectively.

From July to August 2012, he was a Visiting Scholar with George Mason University, VA, USA. From October 2013 to October 2014, he was a Visiting Scholar with the School of Electrical and Computer Engineering, Georgia Institute of Technology, Atlanta, GA, USA. He is currently a Full Professor with the School of Electrical Engineering, Southwest Jiaotong University, and the Vice Director of the Department of Power Electronics and Electrical Drive. He has authored and coauthored more than 60 technical articles. His research interests include stability analysis and control of electric traction systems, fault diagnosis, and hardware-in-the-loop simulation of traction converter and motor drive systems.

SONGTAO LI received the B.Sc. degree in electrical engineering from the Lanzhou University of Technology, Lanzhou, China, in 2018. He is currently pursuing the M.Sc. degree in power electronics and electrical drives with the School of Electrical Engineering, Southwest Jiaotong University, Chengdu, China.

His current research interests include permanent magnet synchronous motor drives and position sensorless control.

MANNAN HASSAN received the B.Sc. and M.Sc. degrees in electronic engineering from the Islamia University of Bahawalpur, Pakistan, in 2012 and 2015, respectively. He is currently pursuing the Ph.D. degree with the School of Electrical Engineering, Southwest Jiaotong University, Chengdu, China.

His research interests include model predictive control, PMSM drives, traction in high-speed railway, and power electronics.